NASA Technical Memorandum 86830

NASA-TM-86830 19860005777

Separated Transonic Airfoil Flow Calculations with a Nonequilibrium Turbulence Model

L.S. King and D.A. Johnson

November 1985

NASA

National Aeronautics and
Space Administration

NF00072

Separated Transonic Airfoil Flow Calculations with a Nonequilibrium Turbulence Model

L. S. King,
D. A. Johnson. Ames Research Center, Moffett Field, California

November 1985

NASA

National Aeronautics and
Space Administration

Ames Research Center
Moffett Field, California 94035

SUMMARY

Navier-Stokes transonic airfoil calculations based on a recently developed
nonequilibrium, turbulence closure model are presented for a supercritical airfoil
section at transonic cruise conditions and for a conventional airfoil section at
shock-induced stall conditions. Comparisons with experimental data are presented
which show that this nonequilibrium closure model performs significantly better than
the popular Baldwin-Lomax and Cebeci-Smith equilibrium algebraic models when there
is boundary-layer separation that results from the inviscid-viscous interactions.

INTRODUCTION

The greatest limiting factor in the accurate numerical prediction of airfoil
flows has been the lack of an adequate turbulence model. For airfoil flows with
sufficiently mild pressure gradients and without separation, simple algebraic turbu-
lence models (e.g., Cebeci and Smith, ref. 1) have been shown to yield good results
(see e.g., refs. 2-4). As speeds are increased into the transonic regime and angles
of attack are increased, however, adverse pressure gradients become stronger, and
separated-flow regions make their appearance. For modern-day supercritical sec-
tions, these problems are further complicated by the high surface curvatures on the
rearward portion of the airfoil. Under these harsher conditions, the algebraic
turbulence models do not work well. Characteristically, they overpredict pressure
recovery on the rearward part of the airfoil. The separated-flow region is pre-
dicted to be much thinner than that observed experimentally, and even the general
shape of the velocity profile in the reverse-flow region does not agree with
experiment.

Recognizing the limitations in the simple algebraic models, considerable effort
has been directed toward incorporating two-equation eddy-viscosity models into
numerical prediction methods. Although these models are more complex, they are also
more general than algebraic models. It was hoped that the greater generality would
provide improved results for high-adverse-pressure-gradient and separated-flow
situations. Indeed, improvements have been noted in predicting the experimentally
observed rapid rise in skin friction downstream of reattachment, and mean-velocity
profiles within the separated region are also in better qualitative agreement with
experiment. Yet, for transonic cases with large separation, the prediction of shock
position and surface pressures has been unsatisfactory (ref. 5).

Recently, a turbulence closure model (ref. 6) designed specifically to treat
two-dimensional, turbulent boundary layers with strong adverse pressure gradients
and attendant separation has been developed. In this model, the influence of

1

history is modeled by using an ordinary differential equation. The equation, derived from the turbulence kinetic-energy equation, describes the streamwise development of the maximum turbulent shear stress. An eddy-viscosity distribution through the inner part of the layer is assumed which has as its velocity scale the maximum turbulent shear stress. In the outer part of the boundary layer, the eddy viscosity is treated as a free parameter which is adjusted to satisfy the Reynolds shear stress resulting from the ordinary differential equation. Because of this, the model is not simply an eddy-viscosity model, but contains features of a Reynolds-stress model.

Results obtained with this new model incorporated into an inverse boundary-layer code were very encouraging (ref. 6). Subsequent to that work, further evalua-tions of this closure model were made (ref. 7) using a compressible Navier-Stokes method. The test flows in this latter study were those developed on the axisym-metric bump wind-tunnel model of reference 8. This wind-tunnel model was designed to produce inviscid-viscous interactions similar to those that develop on airfoils at transonic speeds. In the present work, the closure model has been incorporated into a Navier-Stokes airfoil code so that an assessment of its performance could be made on actual airfoil flows. Two airfoil test flows are considered. The first is the DSMA 671, supercritical airfoil section at test conditions selected to simulate transonic cruise. The second is the NACA 64A010 airfoil section at shock-induced stall conditions. The experimental data for these two test cases are reported in references 9 and 10, respectively.

THE TURBULENCE MODEL

The turbulence closure model as developed in reference 6 has as its basis three main observations: (1) that algebraic models such as the Cebeci-Smith model do quite well for attached flows in mild pressure gradients; (2) that they predict too rapid a rise in turbulent shear stress inside the boundary layer when high adverse-pressure gradients are encountered and, conversely, predict too rapid a decrease in this stress when the pressure gradients are relieved; and (3) that the inner mixing-length formulation of these models results in separated velocity profiles that are inconsistent with experiment.

An algebraic eddy-viscosity distribution

$$\nu_t = \nu_{t_o} (1 - \exp - \nu_{t_i}/\nu_{t_o}) \tag{1}$$

$$\nu_{t_i} = D^2 \, 0.4 \, y(-\overline{u'v'}_m)^{1/2} \tag{2}$$

$$\nu_{t_o} = \sigma(x) \cdot 0.0168 \, U_e \delta_i^* / [1 + 5.5(y/\delta)^6] \tag{3}$$

is used to describe the variation of the Reynolds shear stress normal to the shear layer under both attached and separated-flow conditions. In equation (2), D is a Van Driest-type near-wall damping term, y is the distance normal to the surface, and $-\overline{u'v'}_m$ is the maximum Reynolds shear stress divided by the local density at the given streamwise station. For convenience, $-\overline{u'v'}_m$ will be referred to simply as the maximum Reynolds shear stress. In equation (3), $\sigma(x)$ is an unknown modeling parameter; U_e is the velocity at the edge of the shear layer; δ_i^* is the incompressible boundary-layer displacement thickness; and δ is the boundary-layer thickness. In the model, history effects (i.e., the slow response of the Reynolds shear stresses to local changes in the mean-velocity field) are taken into account through the parameter $\sigma(x)$. The streamwise distribution of this parameter is established in the solution procedure (details are given in ref. 7) to give a streamwise distribution of $-\overline{u'v'}_m$ in the computed flow that satisfies an ordinary differential equation for $-\overline{u'v'}_m$. This O.D.E., which is obtained from simplifications to the turbulence kinetic energy equation, can be found in references 6 and 7.

The model described is designed for wall-bounded shear flows. In the wake, equation (3) was used to represent the eddy viscosities with separate displacement thicknesses used for the upper and lower parts of the wake. These displacement thicknesses were determined by integrating outward from the minimum wake-velocity locations. At the grid points corresponding to the location of minimum velocity, the eddy viscosity was taken to be the average of the eddy viscosities at the upper and lower adjoining grid points. In the wake, $-\overline{u'v'}_m$ decreases with streamwise distance. As a result, $\sigma(x)$ will tend to increase from its value at the trailing edge. When $\sigma(x)$ was less than unity at the trailing edge (this generally will be the case), it was allowed to reach unity downstream but not allowed to exceed unity. If it were greater than 1 at the trailing edge (which would be more likely to occur on the lower airfoil surface), it was set equal to 1 in the wake. Although, initially the eddy viscosities in the upper and lower parts of the wake were unequal, farther downstream the wake was observed to develop symmetry causing the eddy-viscosity distributions also to become symmetric.

In the very-far wake, equation (3) with $\sigma(x) = 1$ underestimates the eddy viscosities by approximately a factor of 4 (ref. 11). However, it seems reasonable that the flow about the airfoil itself should not be sensitive to the very-far-wake development. The treatment of the wake is acknowledged to be very approximate. But in our opinion, the resultant airfoil surface pressures are much more sensitive to the turbulent Reynolds shear-stress development along the airfoil surface than to the rate of decay of these stresses in the wake. The favorable results obtained with this simple wake model support this opinion.

In the two sets of calculations to be presented, a different velocity scale was used for the Van Driest damping term in equation (2). In the DSMA 671 calculations, the conventional friction velocity $u_\tau = (\tau_w/\rho_w)^{1/2}$ was used. But in the NACA 64A010 calculations, steady-state solutions could not be obtained with either the Cebeci-Smith model or the present model when u_τ was used. As in the supersonic compression corner study of reference 12, this problem was alleviated by using

3

$(-\overline{u'v'}_m)^{1/2}$ as the near-wall damping velocity scale. In both sets of calculations, the Van Driest constant, A^+, was taken to be 15.

THE NUMERICAL PROCEDURE

The basic numerical method used in the present investigation is that due to Steger (ref. 13) for the Reynolds-averaged, time-dependent, compressible Navier-Stokes equations. In Steger's method, the governing equations are transformed to a generalized body-fitted coordinate system and solved with the second-order-accurate, factorized implicit algorithm of Beam and Warming (refs. 14 and 15). In the original version of the code, viscous terms in the streamwise direction were neglected, resulting in the so-called "thin-layer approximation." The present version of the code contains all viscous terms, with an implementation similar to that of Degani (ref. 16). To account for wind-tunnel wall interference effects so that direct comparisons with wind-tunnel data may be made, the Steger code has been further modified by incorporating a pressure boundary condition along the upper and lower boundaries. Details of this modification are presented in earlier papers by King and Johnson (refs. 2 and 3).

Mesh generation was accomplished using a Poisson solver similar to that of Thompson et al. (ref. 17) as modified by Steger and Sorenson (ref. 18). The mesh code produces a "wraparound," or C-mesh, and is coincident with user-prescribed points on the boundaries, that is, the airfoil surface and the outer computational boundary. With the Steger-Sorenson modification, orthogonality at the airfoil surface and concentration of coordinate lines near the surface may be controlled to resolve the turbulent boundary layer. In the DSMA 671 calculations, the mesh was composed of 139 points in the wraparound direction and 50 points in the direction away from the airfoil. For the NACA 64A010 calculations, the number of points in the wraparound direction was increased to 159 to ensure adequate resolution of the strong shock-wave/turbulent-boundary-layer interaction of this test case. With this more refined mesh, the streamwise spacing in the vicinity of the shock was approximately 0.01 chord. The meshes were constructed with the first coordinate line off the airfoil at a normal distance of 2×10^{-5} chords from the surface. This distance corresponds roughly to a value of y^+ of 2, with approximately 20 points in the turbulent boundary layer near the airfoil midchord.

The upper and lower mesh boundaries at which measured static pressures were applied as boundary conditions were located at ± 1.125 and ± 1.0 chord for the DSMA 671 and NACA 64A010 sections, respectively. The upstream boundary was located 2 chords upstream of the airfoils. Since no data were available at the upstream boundary, an approximate set of upstream boundary conditions had to be created. For the DSMA 671 airfoil, these were obtained from inviscid free-air calculations (see ref. 2). In the NACA 64A010 calculations, uniform flow at the upstream boundary was assumed.

4

RESULTS AND DISCUSSION

The results obtained for the DSMA 671 airfoil section at test conditions selected to simulate transonic cruise will first be presented. The test conditions were $M_\infty = 0.72$, $\alpha = 4.32°$, and $Re_c = 2.67 \times 10^6$. Transition was initiated on the upper and lower surfaces at $x/c = 0.17$, which corresponds to the transition strip locations of the experiment. The aspect ratio of the airfoil was 3, and the tunnel half-height to chord was 1.5.

The significance of wall effects at these test conditions is illustrated in figure 1, which shows surface-pressure distributions obtained with the Baldwin-Lomax closure model (ref. 19), using free-air and pressure-boundary-conditions. The free-air solution was obtained with the upper and lower boundaries far removed from the airfoil. In order to make comparisons of computations and experiment, it is obvious that the pressure boundary condition (PBC) is necessary. This is also true for the NACA 64A010 test case.

In figure 2, the surface pressures predicted with the present model and with the Baldwin-Lomax model, both using the PBC, are compared with the experimental results. As can be seen, the differences between the solutions of the present model and of the Baldwin-Lomax model are small on the forward portion of the airfoil. The small disagreement with experiment on the forward portion of the airfoil is believed to be a result of the upstream boundary conditions employed. It appears that these boundary conditions created an effective angle of attack that was slightly too large. On the rear portion of the airfoil, high adverse pressure gradients exist because of the high curvature. Separation is predicted to occur slightly forward of that observed in the experiment, at 0.95 chord instead of 0.98 chord. The inset of figure 2, showing the trailing-edge region in greater detail, illustrates that the solution based on the present model is in excellent agreement with the data in this high gradient and separated-flow region. On the other hand, the Baldwin-Lomax model overpredicts pressure recovery in the separated region.

Predicted upper-surface boundary-layer velocity profiles are shown in figure 3 along with the experimental data. Four stations are shown, from $x/c = 0.63$, downstream of the shock, to $x/c = 0.99$, in the separated region. At $x/c = 0.63$, the pressure gradient is small, and the two results agree well with each other and with the data. Proceeding farther downstream, high adverse pressure gradients are encountered, with the result that increasingly larger differences between the two solutions can be seen. At $x/c = 0.99$, the flow is separated. At this streamwise station, the present model results are in good agreement with the experimental data. Such is not the case for the Baldwin-Lomax model results. With this closure model, the momentum loss incurred by the boundary layer at this station is substantially underpredicted, and the shape of the separated profile is not in agreement with the experimental results.

In figure 4, the predicted and measured Reynolds shear-stress profiles are compared at the streamwise stations of the mean-velocity profiles of figure 3. As recommended in reference 7, these results are compared in shear-layer coordinates as

5

defined by the direction of the flow at the location of maximum Reynolds shear stress. The predicted stresses are lower than those measured, but there was concern in the experiment that the measured stresses may have been in error on the high side. This concern arose because $\overline{v'^2}$ was measured to be as large as $\overline{u'^2}$ across the boundary layer at $x/c = 0.63$ and 0.75. Skin-friction determinations from law-of-the-wall fits of the mean-velocity data at these two stations where the stream-wise pressure gradients were small agree better with the predicted shear stresses than with the measured shear stresses, which further suggests that the measured values of $-\overline{u'v'}$ may have been high. Notice from this figure the different rates at which the shear stresses are predicted to increase near the trailing edge for the two closure models. The slower growth in $-\overline{u'v'}$ predicted by the present model accounts for the larger momentum losses and lower pressure recoveries predicted by this model.

As a result of improved velocity predictions with the present model, flow angles in the near-wake are predicted much better than with the Baldwin-Lomax model. The flow angle, $\theta = \arctan \overline{v}/\overline{u}$, is shown in figure 5 along a vertical line in the near-wake 0.02 chord downstream of the trailing edge. In this figure, $y = 0$ corresponds to the vertical position of the airfoil trailing edge. Both the data and the calculations based on the present model show a large jump in flow angle where the boundary-layer flows from the upper and lower surfaces meet.

Velocity profiles in the wake of the supercritical section are shown in figure 6. Because the velocity profiles of the present model were in substantial agreement with the data at the airfoil trailing edge, results in the near-wake also agree well with the data. Farther from the trailing edge, the results from the present model show a larger velocity defect than the data. This is as expected, since the simple wake model employed in the calculation results in eddy-viscosity values which are too low in the far-wake. In contrast to the Baldwin-Lomax model, however, the present model does predict wake position very well.

Results are presented for the NACA 64A010 conventional airfoil in figures 7-10. The test conditions were $M_\infty = 0.8$, $\alpha = 6.2°$, and $Re_c = 2 \times 10^6$. Transition was initiated along the upper and lower surfaces at $x/c = 0.17$, the transition strip locations of the experiment. The aspect ratio was 4 and the tunnel half-height to chord was 2. At these test conditions, the upper-surface boundary layer separates at the shock, and the flow remains separated into the wake. The thick, detached shear layer that develops downstream of the shock is clearly evident in the infinite-fringe interferogram presented in figure 7(a). The fringes represent lines of constant density, which in the inviscid flow regions correspond very nearly to lines of constant Mach number. In figure 7(b), a Mach contour plot of the solution obtained with the present model is presented.

In figure 8, surface-pressure predictions obtained with the present model and with the Cebeci-Smith model are compared with the experimental results. A steady-state solution could not be obtained for this test flow with the Baldwin-Lomax model, so the Cebeci-Smith model (with $(-\overline{u'v'}_m)^{1/2}$ used in the near-wall damping expression) was run instead for comparison purposes. These two algebraic models

6

are, in theory, equivalent (ref. 19). As evident from figure 8, the present model does much better at predicting the resultant pressure distribution for this shock-induced stall condition. The Cebeci-Smith model significantly underpredicts the viscous displacement effects downstream of the shock, as seen from the mean-velocity profile comparisons presented in figure 9. The present model, on the other hand, does quite well at predicting the thick, detached shear layer that is generated by the shock wave farther upstream. Shown alongside the mean-velocity profiles are the predicted and measured Reynolds shear stresses. The calculations and the measurements are compared in shear-layer coordinates as defined by the direction of the flow at the location of maximum Reynolds shear stress. At the two upstream measurement stations, the shear stresses predicted by the present model are in quite good agreement with the experiment. The disagreement between the predicted and measured stresses just downstream of the trailing edge ($x/c = 1.02$) is the result of the approximate wake model. Near the minimum-velocity location, the eddy viscosities are too large, a result of equation (2) being abruptly dropped from the eddy-viscosity relationship immediately downstream of the trailing edge. This deficiency could easily be corrected, for example, by modeling the inner boundary-layer eddy-viscosities approach to the larger wake values to be a function of the wake-velocity deficit.

Shown in figure 10 is the development of $-\overline{u'v'}_m$ with streamwise distance as predicted with the present model and the Cebeci-Smith model. With the present model, a less rapid rise in $-\overline{u'v'}_m$ is predicted to occur at the shock with $-\overline{u'v'}_m$ continuing to grow downstream as a detached shear layer is formed. With the Cebeci-Smith model, however, $-\overline{u'v'}_m$ attained its maximum value at the shock and then monotonically decreased downstream. The decay in $-\overline{u'v'}_m$ downstream of the shock indicates that the computed boundary layer in this case had little difficulty negotiating the larger adverse pressure gradients predicted on the aft section of the airfoil.

CONCLUDING REMARKS

A nonequilibrium turbulence model has been incorporated into a Navier-Stokes airfoil code. Solutions obtained for two different airfoil flows, one with a small trailing-edge separation bubble and the other with a large, shock-induced, detached shear layer, have shown that results with this nonequilibrium model are clearly superior to those obtained with equilibrium models like those of Baldwin and Lomax and Cebeci and Smith. Airfoil surface pressures and boundary-layer and wake-velocity profiles are in much better agreement with experimental data when the nonequilibrium model is used.

REFERENCES

1. Cebeci, T.; and Smith, A. M. O.: Analysis for Turbulent Boundary Layers. Academic Press, New York, 1974.

2. King, L. S.; and Johnson, D. A.: A Note on Transonic Flow Calculations for an Airfoil in a Wind Tunnel. Submitted to AIAA J., 1985.

3. King, L. S.; and Johnson, D. A.: Comparison of Supercritical Airfoil Flow Calculations with Wind Tunnel Results. AIAA Paper 83-1688, Danvers, Mass., 1983.

4. Coakley, T. J.: Turbulence Modeling Methods for the Compressible Navier-Stokes Equations. AIAA Paper 83-1693, Danvers, Mass., 1983.

5. Horstman, C. C.; and Johnson, D. A.: Prediction of Transonic Separated Flows. AIAA J., vol. 22, no. 7, July 1984.

6. Johnson, D. A.; and King, L. S.: A New Turbulence Closure Model for Boundary Layer Flows with Strong Adverse Pressure Gradients and Separation. AIAA Paper 84-0175, Reno, Nev., 1984.

7. Johnson, D. A.: Predictions of Transonic Separated Flow with an Eddy-Viscosity/Reynolds-Shear-Stress Closure Model. AIAA Paper 85-1683, Cincinnati, Ohio, 1985.

8. Bachalo, W. D.; and Johnson, D. A.: An Investigation of Transonic Trubulent Boundary Layer Separation Generated on an Axisymmetric Flow Model. AIAA Paper 79-1479, Williamsburg, Va., 1979.

9. Johnson, D. A.; and Spaid, F. W.: Supercritical Airfoil Boundary-Layer and Near-Wake Measurements. J. Aircraft, vol. 20, Apr. 1983, pp. 298-305.

10. Johnson, D. A.; and Bachalo, W. D.: Transonic Flow past a Symmetrical Airfoil--Inviscid and Turbulent Flow Properties. AIAA J., vol. 18, Jan. 1980, pp. 16-24.

11. Narasimha, R.; and Prabhu, A.: Equilibrium and Relaxation in Turbulent Wakes. J. Fluid Mech., vol. 54, 1972, pp. 1-29.

12. Visbal, M.; and Knight, D.: The Baldwin-Lomax Turbulence Model for Two-Dimensional Shock-Wave/Boundary-Layer Interactions. AIAA J., vol. 22, no. 7, pp. 921-928.

13. Steger, J. L.: Implicit Finite-Difference Simulation of Flow about Arbitrary Two-Dimensional Geometries. AIAA J., vol. 16, July 1978, pp. 679-686.

14. Beam, R.; and Warming, R. F.: An Implicit Finite-Difference Algorithm for Hyperbolic Systems in Conservation-Law Form. J. Comput. Phys., vol. 22, Sept. 1976, pp. 87-110.

15. Beam, R.; and Warming, R. F.: An Implicit Factored Scheme for the Compressible Navier-Stokes Equations. AIAA J., vol. 16, Apr. 1978, pp. 393-402.

16. Degani, D.: Numerical Study of the Effect of an Embedded Surface-Heat Source on the Separation Bubble of Supersonic Flow. AIAA Paper 83-1753, Danvers, Mass., July 1983.

17. Thompson, J. F.; Thames, F. C.; and Mastin, C. M.: Automatic Numerical Generation of Body-Fitted Curvilinear Coordinate System for Field Containing any Number of Arbitrary Two-Dimensional Bodies. J. Comput. Phys., vol. 15, 1974, pp. 299-319.

18. Steger, J. L.; and Sorenson, R. L.: Automatic Mesh-Point Clustering near a Boundary in Grid Generation with Elliptic Partial Differential Equations. J. Comput. Phys., vol. 33, 1979, pp. 405-410.

19. Baldwin, B. S.; and Lomax, H.: Thin-Layer Approximation and Algebraic Model for Separated Turbulent Flows. AIAA Paper 78-257, Huntsville, Ala., 1978.
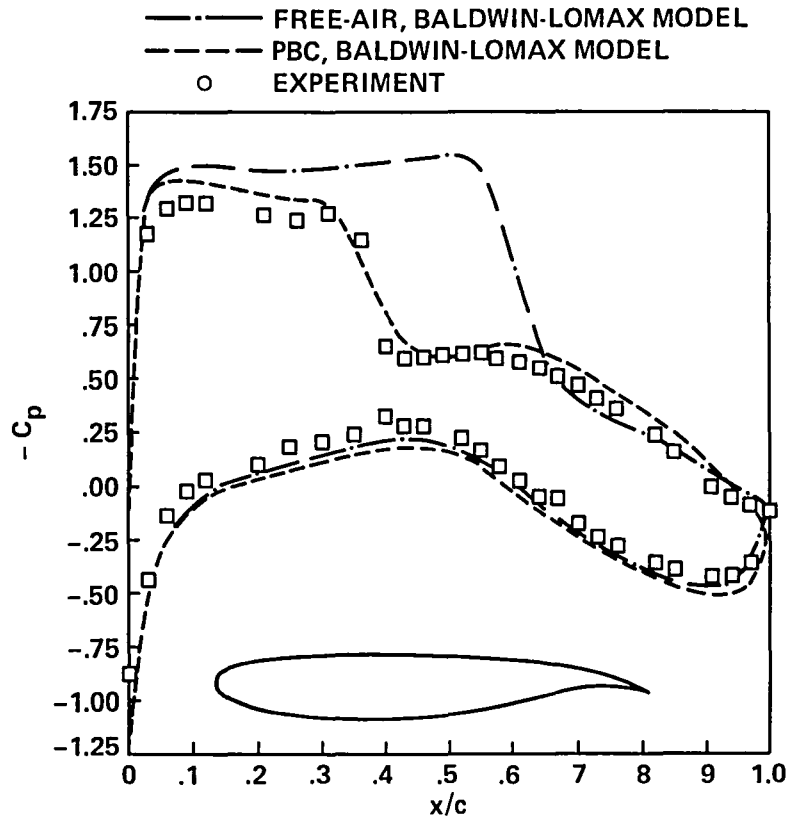
Figure 1.- Comparison of PBC and free-air surface-pressure with experimental results for DSMA 671 supercritical airfoil section: $M_\infty = 0.72$, $\alpha = 4.32°$, $Re_c = 2.67 \times 10^6$.
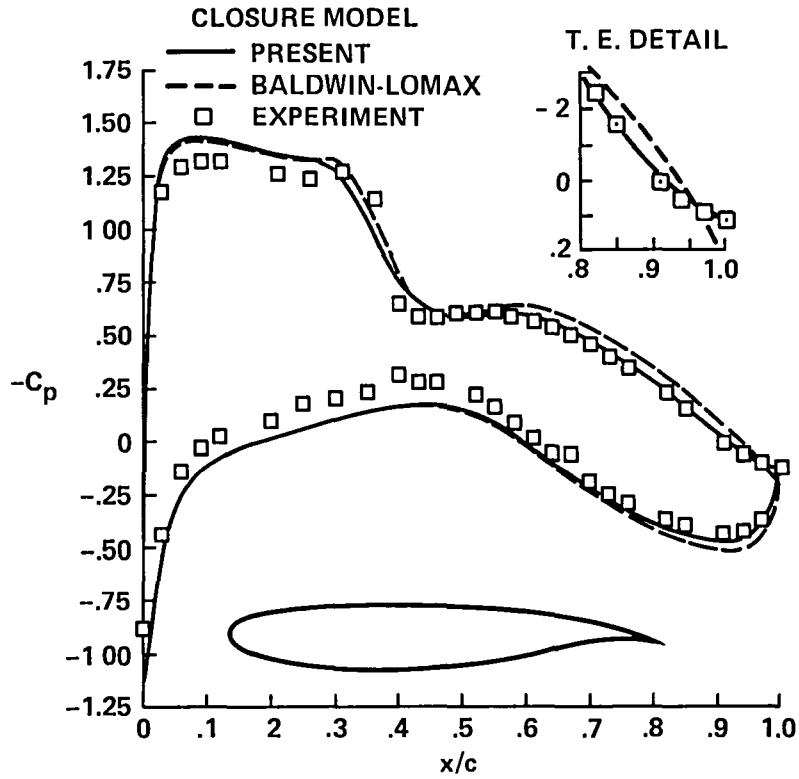
Figure 2.- Comparison of computed and experimental surface pressures: DSMA 671 supercritical airfoil, $M_\infty = 0.72$, $\alpha = 4.32°$, $Re_c = 2.67 \times 10^6$.
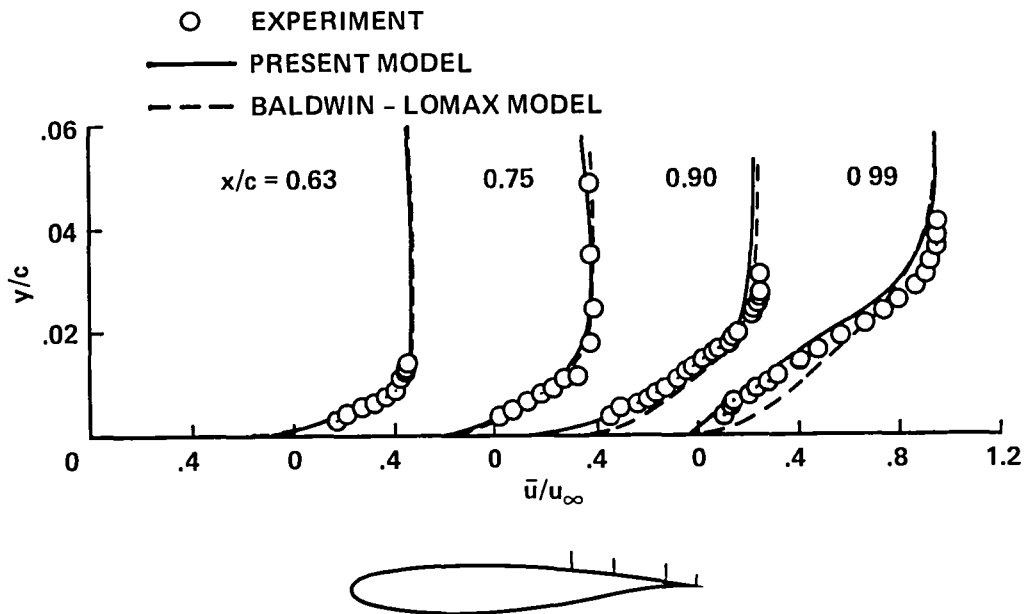

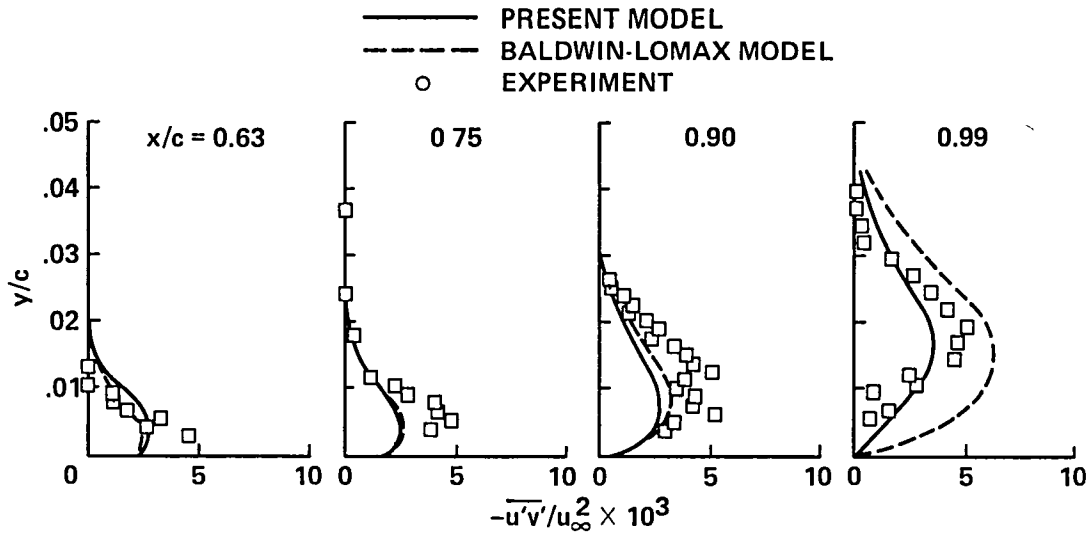Figure 3.- Upper-surface mean-velocity profiles for DSMA 671 section.
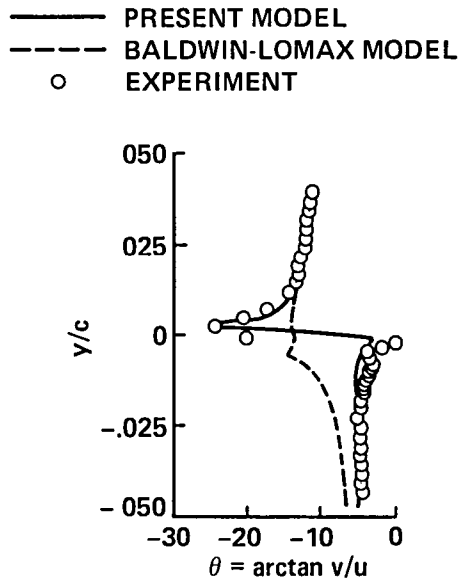
Figure 4.- Upper-surface Reynolds shear-stress profiles for DSMA 671 section.

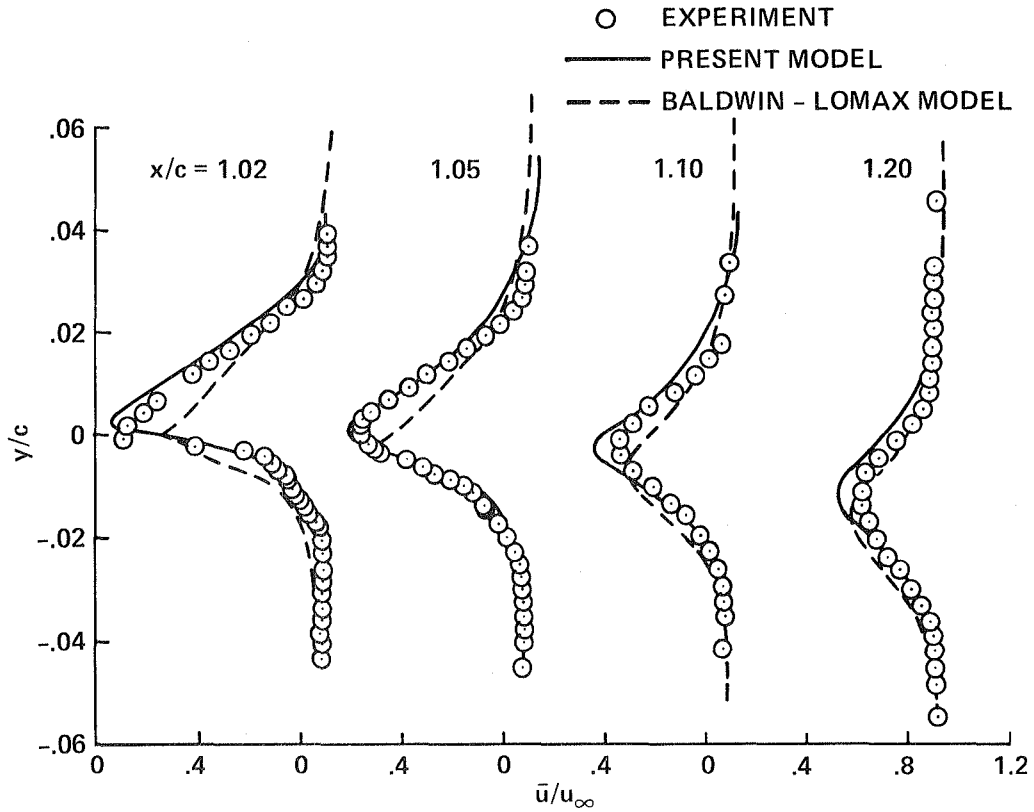
Figure 5.- Flow angles at x/c = 1.02 for DSMA 671 section.
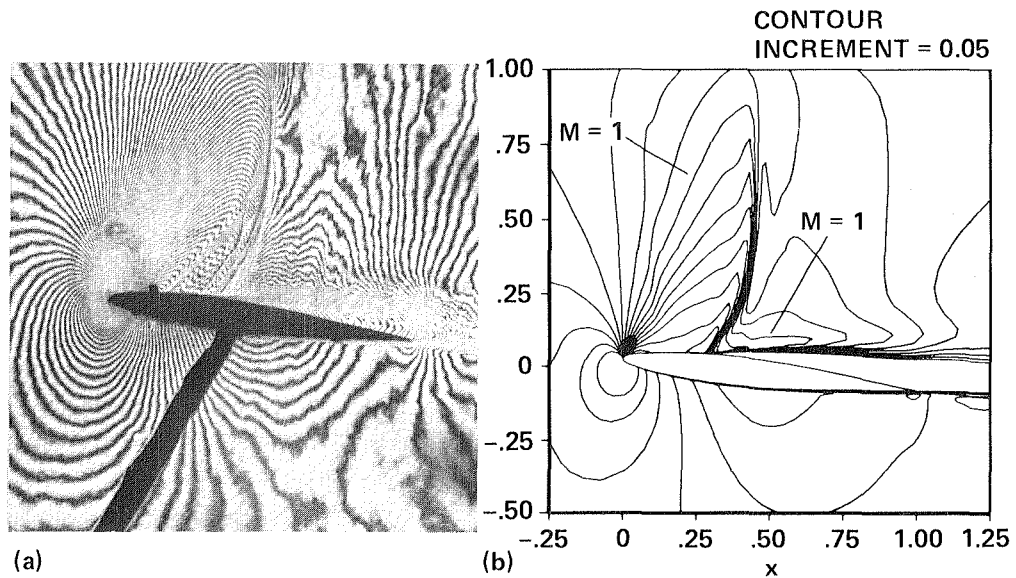
Figure 6.- Mean-velocity profiles in wake of DSMA 671 section.

(a) Infinite-fringe interferogram.

(b) Mach contour plot of computation base on present model.

Figure 7.- NACA 64A010 airfoil section at shock-induced stall conditions: $M_\infty = 0.8$, $\alpha = 6.2°$, $Re_c = 2 \times 10^6$.
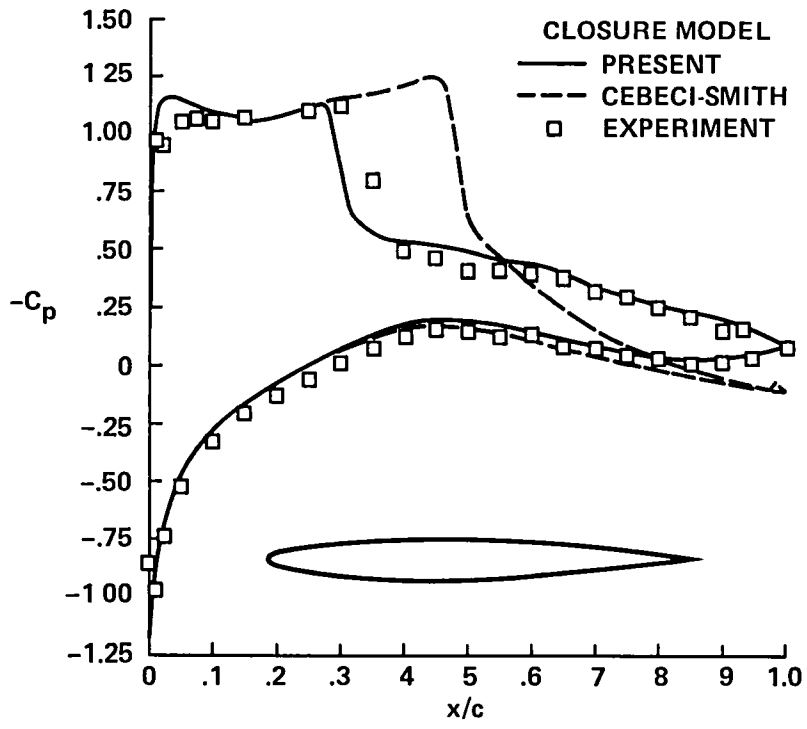
Figure 8.- Comparison of computed and experimental surface pressures for NACA 64A010 airfoil at shock-induced stall conditions: $M_\infty = 0.8$, $\alpha = 6.2°$, $Re_c = 2\times10^6$.
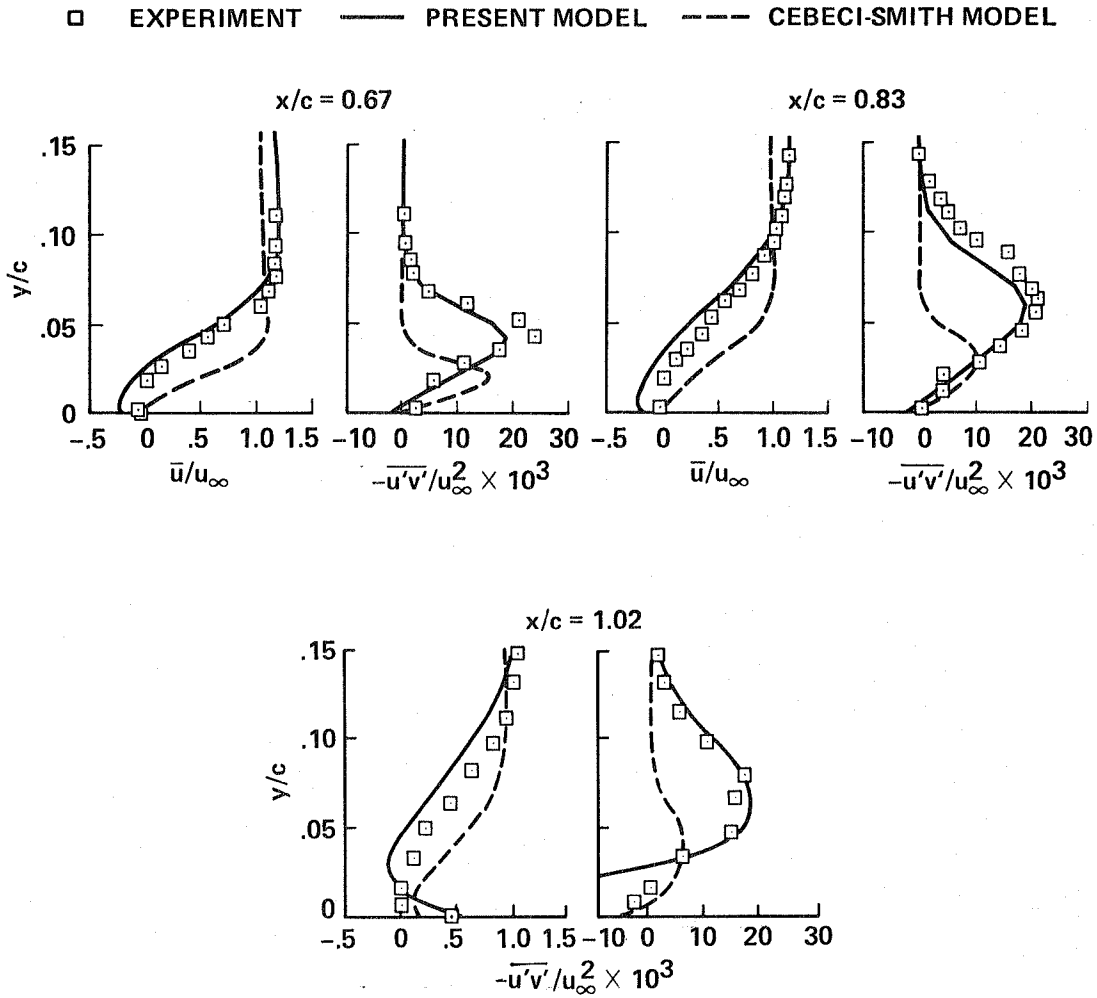
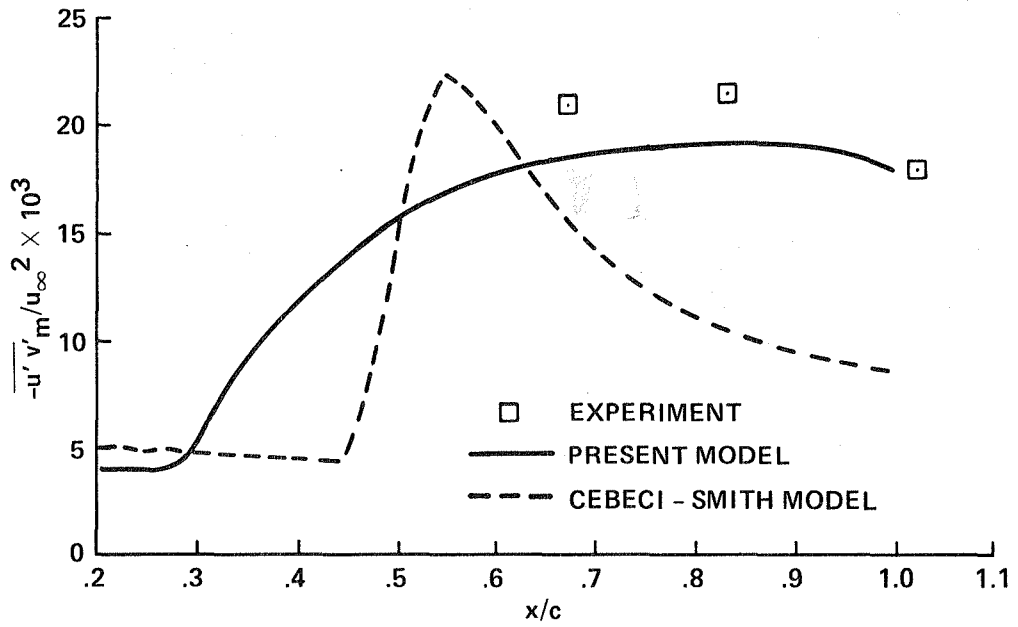Figure 9.- Upper-surface and near-wake mean-velocity and Reynolds shear-stress profiles for NACA 64A010 section.

Figure 10.- Upper-surface maximum Reynolds shear-stress development with streamwise distance for NACA 64A010 section.

1 Report No	2 Government Accession No	3 Recipient's Catalog No
NASA TM-86830		

4 Title and Subtitle	5 Report Date
SEPARATED TRANSONIC AIRFOIL FLOW CALCULATIONS WITH A NONEQUILIBRIUM TURBULENCE MODEL	November 1985
	6 Performing Organization Code

7 Author(s)	8 Performing Organization Report No
L. S. King and D. A. Johnson	A-85397
	10 Work Unit No

9 Performing Organization Name and Address	
Ames Research Center Moffett Field, CA 94035	11 Contract or Grant No
	13 Type of Report and Period Covered

12 Sponsoring Agency Name and Address	
National Aeronautics and Space Administration Washington, DC 20546	Technical Memorandum
	14 Sponsoring Agency Code
	506-51-11

15 Supplementary Notes

Point of contact: D. A. Johnson, Ames Research Center, MS 229-1, Moffett Field, CA 94035, (415) 694-5399 or FTS 464-5399

16 Abstract

Navier-Stokes transonic airfoil calculations based on a recently developed nonequilibrium, turbulence closure model are presented for a supercritical airfoil section at transonic cruise conditions and for a conventional airfoil section at shock-induced stall conditions. Comparisons with experimental data are presented which show that this nonequilibrium closure model performs significantly better than the popular Baldwin-Lomax and Cebeci-Smith equilibrium algebraic models when there is boundary-layer separation that results from the inviscid-viscous interactions.

17 Key Words (Suggested by Author(s))	18 Distribution Statement
Airfoils Transonic flow Turbulent flow Separated flow Turbulence closure	Unlimited Subject category: 02

19 Security Classif (of this report)	20 Security Classif (of this page)	21 No of Pages	22 Price
Unclassified	Unclassified	18	A02

End of Document